

Power quality optimization using a novel backstepping control of a three-phase grid-connected photovoltaic systems

Salwa Naddami, Najib Ababssi

IMII Laboratory, Faculty of Science and Technology, Hassan First University, Settat, Morocco

Article Info

Article history:

Received Jan 19, 2022

Revised Aug 31, 2022

Accepted Sep 2, 2022

Keywords:

Backstepping control

Boost converter

Inverter

Maximum power point

Power quality

Photovoltaic modules

ABSTRACT

A novel nonlinear backstepping controller based on direct current (DC) link voltage control is proposed in three-phase grid-connected solar photovoltaic (PV) systems to control the active and reactive power flow between the PV system and the grid with improved power quality in terms of pure sinusoidal current injection with lower total harmonic distortion (THD), as well as to ensure unity power factor, or to compensate for reactive power required by the load, i.e., the electrical grid. The output power of the PV array is supplied to the grid through a boost converter with maximum power point tracking (MPPT) control and an inverter. Simulation results of the proposed controller show good robustness under nominal conditions, parameter variations, and load disturbances, which presents the main advantage of this controller as compared to an existing controller. The performance of this work was evaluated using a MATLAB/Simulink environment.

This is an open access article under the [CC BY-SA](https://creativecommons.org/licenses/by-sa/4.0/) license.



Corresponding Author:

Salwa Naddami

IMII Laboratory, Faculty of Science and Technology, Hassan First University

Settat 26000, Morocco

Email: salwa.naddami@gmail.com

1. INTRODUCTION

Currently, a trend of rapid growth in energy needs has been observed in the world. As a result, most countries are using renewable energy resources (RES) to generate electricity. A new development is the integration of RES, such as wind and solar energy, into the power grid at the distribution level [1]. These distributed energy resources inject electrical energy directly through a solar or wind system based on power electronic converters [2], [3]. The topology of a photovoltaic (PV) system is classified into two categories: The first type is a single-stage PV system [4]–[6], in which the grid is connected directly to the PV sources via a direct current/alternating current (DC/AC) inverter to achieve maximum power point tracking and unity power factor (UPF). The second type is a two-stage PV system [7]–[9], in which the PV panels are connected to the grid via a DC/DC boost power converter that operates with an maximum power point tracking (MPPT) and a DC/AC inverter to achieve UPF. In this work, a two-stage power conversion was used in the grid system. Therefore, photovoltaic solar systems are composed of a solar module array, a DC-DC power converter, and a DC-AC inverter as the final interface [10], [11].

The objective of the main control of grid-connected photovoltaic systems is to extract the maximum power from the PV and inject the active and reactive power to the grid within the maximum available power while improving the quality of the delivered power [12]. Traditional linear controllers [13]–[15], are frequently employed because of their simplicity construction and versatility in solving a variety of practical control problems. However due to the nonlinearities of grid-connected photovoltaic systems, in the presence of parametric uncertainties, sudden disturbances, weather conditions, or load changes; the desired values may not be followed

in a wide range of operational regions when using linear controllers. Consequently, nonlinear control strategies are deployed to conquer the operating point limitation of grid-connected photovoltaic systems [16], [17].

In the literature review of grid-connected photovoltaic systems, there are several studies have been conducted. Lalili *et al.* [18], propose the feedback linearizing (FBL) technique to eliminate innate nonlinear effects in photovoltaic system by converting the system to partially or totally linearized one. However, these feedback linearization controllers are extremely sensitive to parameter variations. In [19], [20], the authors suggest the sliding mode controller, which guarantees the satisfaction of the control objectives even in the presence of nonlinearities, model parameter fluctuations, and external disturbances. However, oscillations are caused by high frequency switching and can reduce the output power due to chattering phenomenon [21].

A backstepping controller based on the Lyapunov function overcomes some of the drawbacks of a feedback linearization controller by considering the complete nonlinearities of the system. In [22], [23], the authors propose the design of a backstepping controller for the nonlinear behavior of the switching current on the inverter side to control only the active power while ensuring a unit power factor (UPF) with the reactive power assumed to be zero. However, this control method was not able to achieve the objectives with good performance under the constraints of the PV system (climate changes, parametric uncertainties, and load change). Furthermore, the reactive power demanded by the load must be provided by the power grid or by external compensation devices, which is extremely costly.

For this reason, the aim of the present study is to develop a new backstepping controller based on DC link voltage control as in [24], to meet the control objectives of ensuring maximum power extraction and controlling the active and reactive power flow between the PV system and the grid, as well as improving power quality by injecting sinusoidal current with low harmonic distortion, even in the presence of parameter variation and external disturbances. This method can eliminate the limitations of the existing controllers by optimizing the PV system dynamic responses, controller robustness, and stability performance. The rest of the work is structured as follows: first, a description of the system and a dynamic model are presented in section 2. In section 3, the design of the controller strategy of the boost converter and the three-phase AC inverter. Section 4 is devoted to the simulation results with different analyses. Lastly, the conclusion is formulated.

2. MODELING OF 100 kW GRID-CONNECTED PV SYSTEM

The primary step in the suggested backstepping design strategy is to develop a non-linear mathematical model of the three-phase grid-connected solar PV system, as illustrated in Figure 1. The configuration of This system contains: PV array, DC converter, DC link capacitor, three-phase voltage source inverter (VSI) consists of six power insulated-gate bipolar transistor (IGBT) switches, inductive filter, and grid. The PV voltage is connected to the DC-link capacitor through the boost converter. The output voltage of the inverter connects to the grid via an RL filter. (e_a, e_b, e_c); (i_a, i_b, i_c); (V_a, V_b, V_c) are respectively three phase-grid voltages, injected currents, and three-phase inverter voltages. V_{dc} is the DC link voltage; V_{pv}, i_{pv} are respectively the PVG voltage and current.

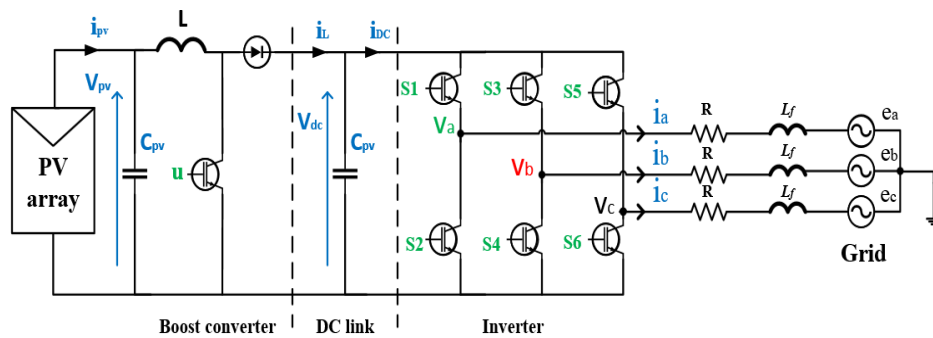


Figure 1. Three phase grid connected PV system

2.1. Photovoltaic array model

The equation that defines the voltage-current characteristic is as (1) [25],

$$I_{pv} = I_{ph} - I_s \left(e^{\frac{V_{pv} + R_s I_{pv}}{aV_t}} - 1 \right) - \frac{V_{pv} + R_s I_{pv}}{R_{sh}} \tag{1}$$

where I_{pv} and I_s are respectively photo current and cell saturation of dark current. V_t is Thermal voltage which is $V = kT/q$. where $q = 1.6 \times 10^{-19}$ C charge of an electron. T is the cell's working temperature, and a is an ideality factor. The R_p and R_s are respectively Shunt or parallel resistance and Series resistance.

The PV array is formed by the association of a predetermined number of 215 Wp panels, in series to form strings that set the required voltage, then the strings are interconnected in parallel to determine the current of the renewable source. In the presented system the PV farm is composed of 47 strings in parallel, each string is composed of 10 modules in series.

2.2. DC-DC Converter modeling

A DC-DC boost converter is employed as an interface between the DC bus and the PV array to monitor the MPP for different irradiation and climatic conditions. The duty cycle of the converter switch is always set with MPPT algorithms to keep the solar panel operating continuously at MPP. The boost converter's control input u is a PWM signal with values in the range $\{0,1\}$. By application of Kirchhoff's laws successively with $u = 1$ and $u = 0$ to the boost converter circuit, the dynamic equations can be formulated as (2) and (3) [26]:

$$\frac{dV_{pv}}{dt} = \frac{1}{C_{pv}} I_{pv} - \frac{1}{C_{pv}} i_L \quad (2)$$

$$\frac{di_L}{dt} = \frac{1}{L} V_{pv} - \frac{1}{L} (1-u) V_{dc} \quad (3)$$

2.3. DC-AC inverter modeling

The three-phase inverter is used to transform the voltage from DC to three-phase AC voltage [27]. To connect the inverter to the grid, the AC voltage of the PV generator, must be synchronized with the grid voltage by using phase-locked loop (PLL) method [28]. According to the Kirchhoff equations of the elementary circuits, and after the Park transformation, we obtain the VSI equations from the circuit and the representation in the DQ frame as (4),

$$\begin{cases} V_a = Ri_a + L_f \frac{di_a}{dt} + e_a \\ V_b = Ri_b + L_f \frac{di_b}{dt} + e_b \\ V_c = Ri_c + L_f \frac{di_c}{dt} + e_c \end{cases} \begin{cases} V_d = RI_d + L_f \frac{dI_d}{dt} + L_f \omega I_q + E_d \\ V_q = RI_q + L_f \frac{dI_q}{dt} - L_f \omega I_d + E_q \end{cases} \quad (4)$$

where: $\begin{pmatrix} V_d \\ V_q \\ V_0 \end{pmatrix} = K \begin{pmatrix} V_a \\ V_b \\ V_c \end{pmatrix}$; $\begin{pmatrix} E_d \\ E_q \\ E_0 \end{pmatrix} = K \begin{pmatrix} e_a \\ e_b \\ e_c \end{pmatrix}$; $\begin{pmatrix} I_d \\ I_q \\ I_0 \end{pmatrix} = K \begin{pmatrix} i_a \\ i_b \\ i_c \end{pmatrix}$

$$\text{and } K = \frac{2}{3} \begin{pmatrix} \cos(\omega t) & \cos(\omega t - 120^\circ) & \cos(\omega t + 120^\circ) \\ -\sin(\omega t) & -\sin(\omega t - 120^\circ) & -\sin(\omega t + 120^\circ) \\ \frac{1}{2} & \frac{1}{2} & \frac{1}{2} \end{pmatrix}$$

By considering a lossless power conversion system, the concept of power balance between the dc input side and the ac output side can be rewritten (5).

$$P_{dc} = P_g \quad V_{dc} i_{dc} = \frac{2}{3} E_d I_d \quad (5)$$

The capacitor across the DC-link voltage dynamics can be written as (6) and (7),

$$C_{dc} \frac{dV_{dc}}{dt} = i_L - i_{dc} \quad \text{where: } i_{dc} = \frac{2}{3} \frac{E_d}{V_{dc}} I_d \quad (6)$$

$$\frac{dV_{dc}}{dt} = \frac{1}{C_{dc}} \left(i_L - \left(\frac{2}{3} \right) \frac{E_d}{V_{dc}} I_d \right) \quad (7)$$

The state equation of the VSI system can be represented (8) to (10).

$$\frac{dV_{dc}}{dt} = \frac{1}{C_{dc}} \left(i_L - \frac{3}{2V_{dc}} E_d I_d \right) \quad (8)$$

$$\frac{dI_d}{dt} = \omega I_q - \frac{R}{L_f} I_d - \frac{E_d}{L_f} + \frac{V_d}{L_f} \tag{9}$$

$$\frac{dI_q}{dt} = -\omega I_d - \frac{R}{L_f} I_q - \frac{E_q}{L_f} + \frac{V_q}{L_f} \tag{10}$$

where (V_d, V_q) is the input control vector.

2.4. Backstepping controller design

Three controllers are synthesized in this work: a PV voltage controller, a DC link capacitor voltage controller, and a current controller: the first controller consists of a loop to determine the MPPT, and the second controller consists of an external loop that helps maintain the DC bus voltage at a given reference and an internal loop that controls the grid current, while the third controller is responsible for transferring the appropriate reactive power to the grid. The backstepping controller strategy was adopted because it has demonstrated high performance and robustness in the presence of parameter fluctuations and disturbances.

The block diagram in Figure 2 illustrates the controller simulation. The inverter currents ($I_a, I_b,$ and I_c) and grid voltages ($E_a, E_b,$ and E_c) are converted in the DQ axis to $I_d, I_q, E_d,$ and E_q and subjected to backstepping control. The photovoltaic voltage (V_{pv}) and current (I_{pv}) are also used to perform the MPPT technique, which produces references that are sent to the system controller input.

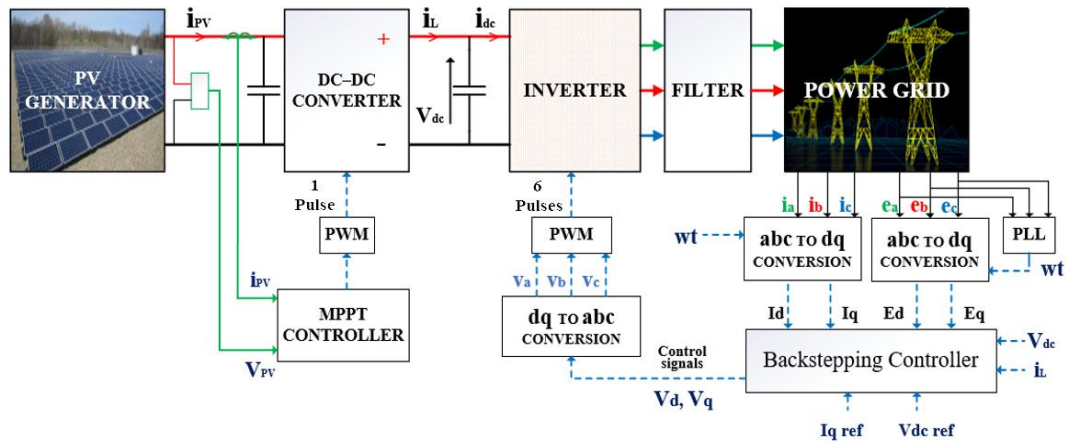


Figure 2. Control scheme of the proposed PV system

2.4.1. MPPT control strategy for boost converter

To meet the maximum power extraction requirement and ensure effective energy transfer from the solar panels to the grid, a nonlinear controller using the backstepping approach is used. The output voltage of the panels converges to the V_{ref} value provided by the MPPT controller, allowing the PV array to extract its maximum power under various weather conditions. The equations synthesis needed for backstepping control of the boost converter are shown in (2) and (3).

Step 1: Set the first tracking error and its derivative as (11).

$$\mathcal{E}_1 = V_{pv} - V_{ref}, \dot{\mathcal{E}}_1 = \frac{1}{C_{pv}} i_p - \frac{1}{C_{pv}} i_L - \dot{V}_{ref} \tag{11}$$

Introduction of Lyapunov function and time derivative (12).

$$V_1(\mathcal{E}_1) = \frac{1}{2} \mathcal{E}_1^2, \dot{V}_1(\mathcal{E}_1) = \mathcal{E}_1 \dot{\mathcal{E}}_1 = \mathcal{E}_1 \left(\frac{1}{C_{pv}} i_p - \frac{1}{C_{pv}} i_L - \dot{V}_{ref} \right) \tag{12}$$

A virtual control αI must be introduced to stabilize the tracking error to the origin. Where αI is the desired inductor current value, it is described as: $\alpha_1 = (iL)_d$. Consequently, to force the derivative of the Lyapunov function to be negative, the virtual control law must realize the (13).

$$\alpha_1 = I_{pv} + C_{pv} (C_1 \mathcal{E}_1 - \dot{V}_{ref}) \tag{13}$$

The judicious choice of α_1 leads to write $\dot{\mathcal{E}}_1 = -C_1 \mathcal{E}_1$

$$\dot{V}_1(\mathcal{E}_1) = -C_1 \mathcal{E}_1^2 \quad \text{This guarantees the stability of the system}$$

Step 2: The second tracking error that represents the difference between the state variable iL and its desired value α_1 is:

$$\mathcal{E}_2 = I_L - \alpha_1 \quad (14)$$

By using (3), the time derivative of the second tracking error can be expressed as (15).

$$\dot{\mathcal{E}}_2 = \frac{1}{L} V_{pv} - \frac{1}{L} (1-u) V_{dc} - \dot{\alpha}_1 \quad (15)$$

The new function of Lyapunov and its derivative can be expressed as (16) to (18),

$$V_2(\mathcal{E}_1, \mathcal{E}_2) = V_1 + \frac{1}{2} \mathcal{E}_2^2 \quad (16)$$

$$\dot{V}_2(\mathcal{E}_1, \mathcal{E}_2) = \mathcal{E}_1 \dot{\mathcal{E}}_1 + \mathcal{E}_2 \dot{\mathcal{E}}_2, \quad \dot{V}_2 = -C_1 \mathcal{E}_1^2 + \mathcal{E}_2 \left[-\left(\frac{1}{C_p}\right) \mathcal{E}_1 + \frac{1}{L} V_{pv} - \frac{1}{L} (1-u) V_{dc} - \dot{\alpha}_1 \right] \quad (17)$$

$$\text{where: } \dot{\mathcal{E}}_1 = \frac{1}{C_{pv}} i_p - \frac{1}{C_{pv}} (\alpha_1 + \mathcal{E}_2) - \dot{V}_{ref} \quad (18)$$

The command u is chosen to obtain the expression (19).

$$-\frac{1}{C_p} \mathcal{E}_1 + \frac{1}{L} V_{pv} - \frac{1}{L} (1-u) V_{dc} - \dot{\alpha}_1 = -C_2 \mathcal{E}_2 \quad (19)$$

As a result, the expression for the command u that the backstepping controller must generate is:

$$u = \frac{L}{V_{dc}} \left[-C_2 \mathcal{E}_2 + \frac{1}{C_p} \mathcal{E}_1 - \frac{1}{L} (V_p - V_{dc}) + \dot{\alpha}_1 \right] \quad (20)$$

Hence the error variables (\mathcal{E}_1 , \mathcal{E}_2) converge asymptotically to the origin, implying that V_{pv} converges asymptotically to the reference value V_{ref} , producing the maximum power from the PV system.

2.4.2. Control of active and reactive power of grid side

To inject the maximum total power extracted from the PV array into the grid and to regulate the reactive power, the control of the AC inverter is performed in a cascade approach by controlling both the DC link voltage and the grid currents. The expression for the active and reactive power can be written as follows assuming the q-axis component (E_q) is zero:

$$P = \frac{3}{2} (E_d I_d + E_q I_q), \quad P = \frac{3}{2} E_d I_d \quad (21)$$

$$Q = \frac{3}{2} (E_d I_q - E_q I_d), \quad Q = -\frac{3}{2} E_d I_q \quad (22)$$

The voltage control inputs V_d and V_q must be generated in such a way that the state trajectories of V_{dref} and the current I_{qref} can be tracked through the control actions of V_{dc} and I_q , i.e., their tracking errors must converge to the origin, in order to inject the suitable active and reactive power into the grid with reduced harmonic distortion.

Step 1: The tracking error between the actual and desired DC link voltage values is given as:

$$\mathcal{E}_3 = V_{dc} - V_{dcref} \quad (23)$$

The time derivative of the tracking error $\dot{\mathcal{E}}_3$ can be expressed as using (8):

$$\dot{\mathcal{E}}_3 = \frac{1}{C_{dc}} (i_L - \frac{3}{2V_{dc}} E_d I_d) \quad (24)$$

The Lyapunov candidate function (LCF) and its derivatives can be written as (25).

$$V_3 = \frac{1}{2} \mathcal{E}_3^2, \quad \dot{V}_3 = \mathcal{E}_3 \dot{\mathcal{E}}_3 = \mathcal{E}_3 \left(\frac{i_L}{C_{dc}} - \frac{3}{2V_{dc}} E_d I_d \right) \quad (25)$$

To stabilize the tracking error \mathcal{E}_3 to zero, the virtual value of I_d needs to be selected in such a way that $\dot{V}_3 < 0$. If the virtual value of I_d is α_2 , it can be chosen as (26).

$$\alpha_2 = (I_d)_d, \quad \alpha_2 = \frac{2C_{dc}V_{dc}}{3E_d} \left(C_3 \mathcal{E}_3 + \frac{i_L}{C_{dc}} \right) \quad (26)$$

This selection of the virtual control input α_2 ensures that (24) yields a negative semi-definite function, as illustrated in equation: $\dot{V}_3 = -C_3 \mathcal{E}_3^2$. The dynamic of the virtual control input (α_2) will be utilized in the next step.

Step 2: The virtual control α_2 is not equal to the d-axis current in the first step, there is an error between them to correct this error, another tracking error for the d-axis current and its derivative can be defined as (27).

$$\mathcal{E}_4 = I_d - \alpha_2, \quad \dot{\mathcal{E}}_4 = wI_q - \frac{R}{L_f} I_d - \frac{E_d}{L_f} + \frac{V_d}{L_f} - \dot{\alpha}_2 \quad (27)$$

The Lyapunov candidate function and the time derivative can be defined as (28).

$$V_4 = \frac{1}{2} \mathcal{E}_4^2 + V_3, \quad \dot{V}_4 = \mathcal{E}_4 \dot{\mathcal{E}}_4 + \dot{V}_3 \quad (28)$$

Substituting the (27) and (25) into (28), The time derivative of the LCF can be written as (29).

$$\dot{V}_4 = -C_3 \mathcal{E}_3^2 + \mathcal{E}_4 \left[-\frac{3}{2V_{dc}} E_d + wI_q - \frac{R}{L_f} I_d - \frac{E_d}{L_f} + \frac{V_d}{L_f} - \dot{\alpha}_2 \right] \quad (29)$$

\dot{V}_4 should be negative to ensure the stability of this subsystem, so: $\dot{V}_4 = -C_3 \mathcal{E}_3^2 - C_4 \mathcal{E}_4^2$. The dynamics of tracking errors of V_{dc} and d-axes current can be stabilized by designing the control law V_d as (30).

$$V_d = L_f \left[-C_4 \mathcal{E}_4 + \frac{3}{2V_{dc}} E_d - wI_q + \frac{R}{L_f} I_d + \dot{\alpha}_2 \right] \quad (30)$$

Step 3: Reactive power control

The desired reactive power can be expressed as [29]: $Q_{ref} = -\frac{3}{2} E_d I_{qref}$. The inverter should supply the required reactive power. As a result, the tracking error and its derivative for the q-axis current using the (10) can be written as (31).

$$\mathcal{E}_5 = I_q - I_{qref}, \quad \dot{\mathcal{E}}_5 = -wI_d - \frac{R}{L_f} I_q - \frac{E_q}{L_f} + \frac{V_q}{L_f} - \dot{I}_{qref} \quad (31)$$

The time derivative of the Lyapunov candidate function corresponding to \mathcal{E}_5 is as (32):

$$\dot{V}_5 = \mathcal{E}_5 \left[-wI_d - \frac{R}{L_f} I_q - \frac{E_q}{L_f} + \frac{V_q}{L_f} - \dot{I}_{qref} \right] \quad (32)$$

\dot{V}_5 should be negative as follows to ensure the stability of this subsystem, so: $\dot{V}_5 = -C_5 \mathcal{E}_5^2$. The control law V_q can be expressed as

$$V_q = L_f \left[wI_d + \frac{R}{L_f} I_q + \frac{E_q}{L_f} + \dot{I}_{qref} - C_5 \mathcal{E}_5 \right] \quad (33)$$

After obtaining the control input V_d and V_q ; three modulating signals V_a , V_b , and V_c , are generated after performing the inverse Park transformation from DQ to ABC. These three modulating signals will generate six switching pulses for the inverter using the PWM generator as illustrated in Figure 2. For positive gain parameters, all Lyapunov expressions are negative semi-definite functions.

3. SIMULATION RESULT

To evaluate the performance of the proposed nonlinear controller, numerical simulations are performed on the Simulink/MATLAB platform. The model contains two power converters that connect the photovoltaic panel to the grid via an L-filter. The parameters of the photovoltaic system components and the controller are shown in Table 1.

The control objectives will be achieved to produce 100 kW of active power and 50 kVAR of reactive power; the amount of power injected depends on the output power of the PV array and the required power factor. The output of the boost converter, which maintains a constant voltage of 600 V through the MPPT system, is sent to the DC link capacitor. This DC voltage is converted to a 400 V AC voltage via a three-phase inverter. The inverter is connected to the grid via a 1 MVA, 400 V/20 kV transformer. To verify the performance of the new nonlinear backstepping controller, the comparison is made with an existing controller. The following operating conditions are considered:

Table 1. Parameters of the boost, inverter, and implemented controllers

Boost converter, inverter and grid components and values		Controllers' parameters	
C _{pv} (PV capacitor)	3500 μ F	Boost	C1 = 1000
L (boost inductor)	1 mH	Backstepping controller	C2 = 100000
C _{dc} (DC bus capacitor)	3300 μ F	Inverter	C3 = 10000
F _{sw} (Boost switching frequency)	5 kHz	Backstepping controller	C4=10000 C5=100000
R _f (filter resistor)	1 Ω		
V _{dc_ref} (DC bus voltage reference)	600 V		
F _{pwm} (inverter PWM frequency)	10 kHz		
U (RMS L-L, grid voltage)	400 V		
F (Grid frequency)	50 Hz		
P _{load} (load active power)	70 kW		
Q _{load} (load reactive power)	50 KVAR		

3.1. Case 1: Controller performance under standard atmospheric conditions

In this scenario, the PV systems are simulated under normal conditions, with a solar irradiation value set to 1,000 W/m² and an ambient temperature set to 25 °C. The main objective is to inject the maximum power 100 kW with a unit power factor. Figure 3 shows that the DC link voltage has reached the required value 600 v, ensuring maximum power extraction from the panels. Figure 3 also shows that the DC link voltage of the proposed controller tracks the reference voltage more accurately and with less fluctuation than the existing controller.

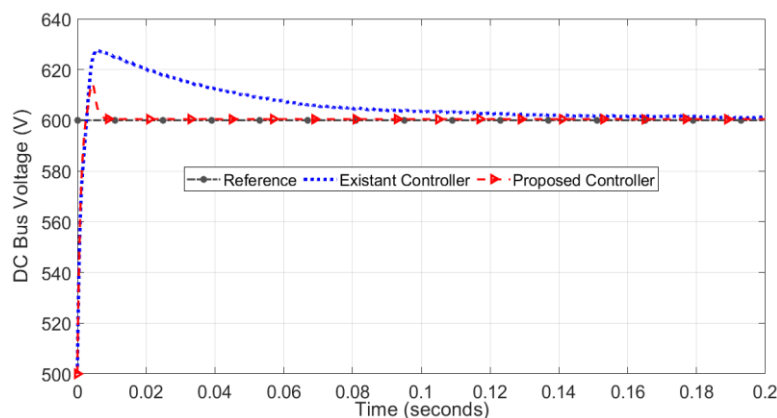


Figure 3. DC link voltage under standard atmospheric conditions

Figure 4(a) shows that the voltage and current are in phase with the proposed and existing backstepping controls, confirming the UPF. Figure 4(b) also shows that when the proposed new controller is used, the output current is extremely close to a pure sine waveform with few harmonic components, while the output current of the existing controller has considerable harmonic components.

To further demonstrate the effectiveness of the proposed method, the fast Fourier transform (FFT) analysis of the grid current with both controllers is shown in Figures 5(a) and 5(b). The THD of the grid current is about 1.75% when the existing control is used; the THD is about 0.88% with the new controller. Figure 6 shows that the maximum power generated by the PV panels is fully injected into the grid when both controllers are used, but the proposed controller has fewer fluctuations than the existing controller.

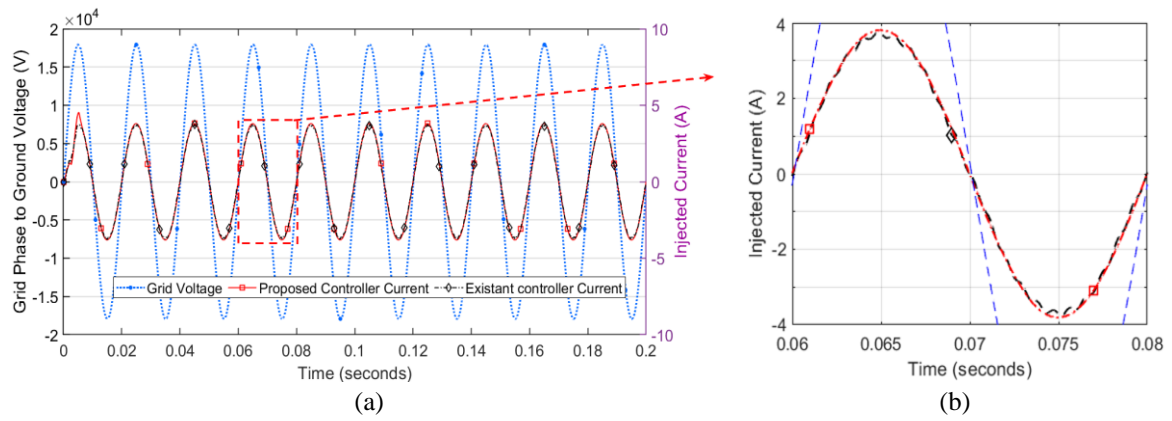


Figure. 4 Grid voltage and injected currents of phase A: (a) waveforms when using the existing and proposed controllers under standard atmospheric conditions and (b) zoomed portion of the injected current

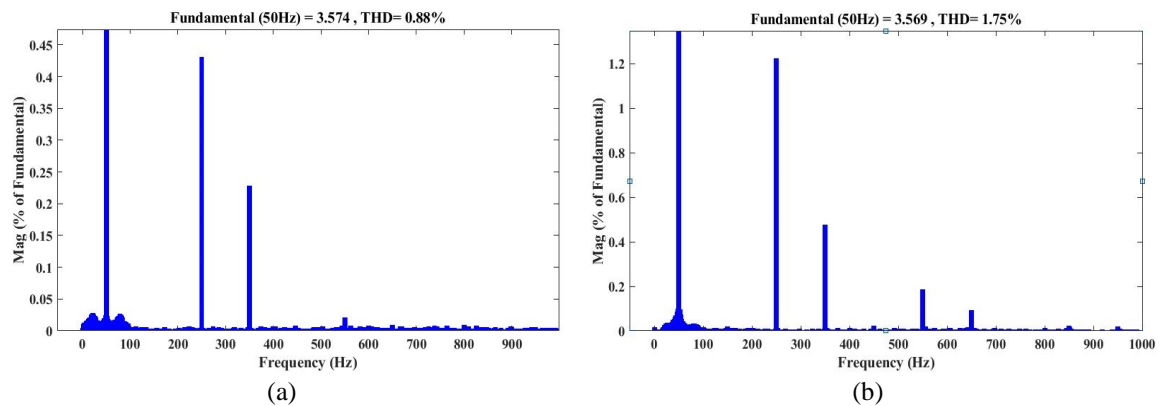


Figure 5. Harmonics of the grid current (a) THD with proposed controller and (b) THD with existing controller

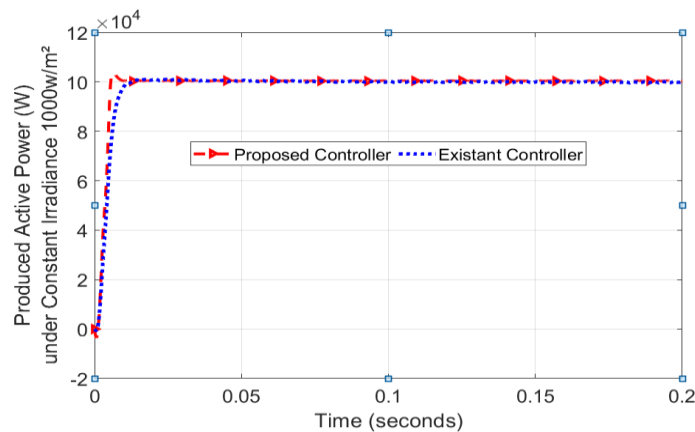


Figure 6. Active power injected into the grid under standard atmospheric conditions

3.2. Case 2: Controller performance under changes in solar irradiation

In this case study, we consider the variation of irradiance while maintaining a constant temperature of 25 °C. In Figure 7(a), the specific irradiance protocol is developed. The initial solar irradiance is assumed to be 500 W/m². After t = 0.065 s, the irradiance increases to 1,000 W/m² and remains there until t = 0.13 s. Finally, after t = 0.13 s, the irradiance decreases from 1,000 to 800 W/m².

Figure 7(b) shows that the DC bus voltage, when the new controller is used, has better tracking capability than the existing controller, it can also be seen that this voltage contains very small overshoots compared to the existing controller. Figure 8 shows that the grid current varies as the irradiance changes. The grid current waveform with the proposed controller is smoother than the response with the existing controller.

The maximum power injected into the grid will start to change from t = 0 s to t = 0.065 s, and from t = 0.065 s to t = 0.2 s, depending on the irradiance changes as shown in Figure 9. The designed controller can inject the amount of active power into the grid with less overshoot compared to the existing controller.

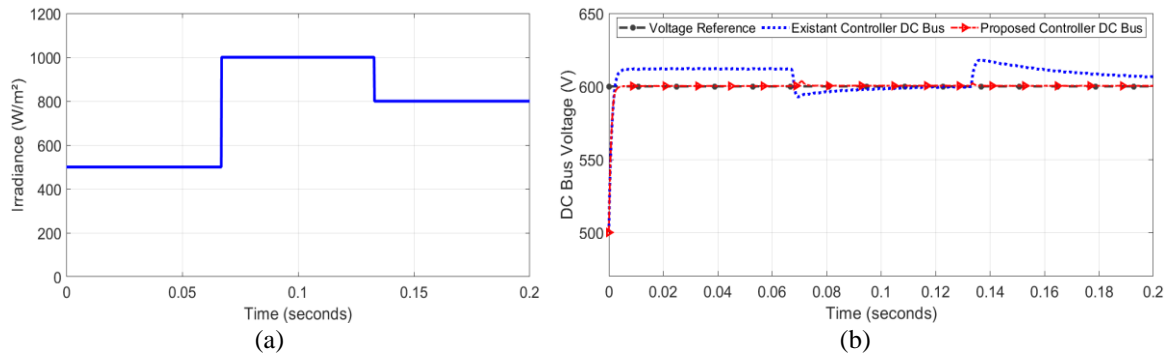


Figure 7. The proposed controller's DC link voltage in comparison to the existing controller: (a) irradiation pattern and (b) DC link voltage under irradiation variation

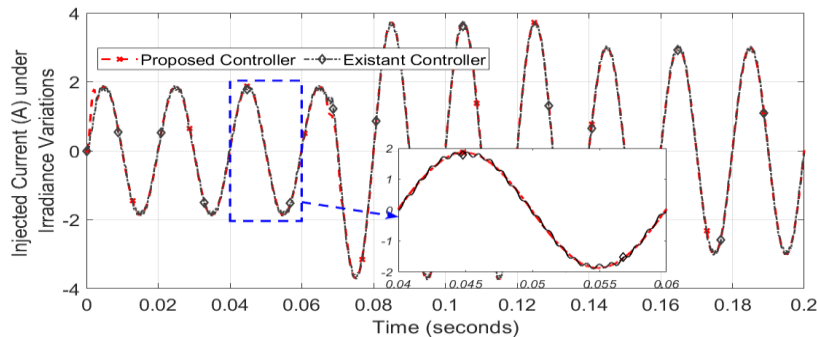


Figure 8. Injected currents with changes in solar irradiation

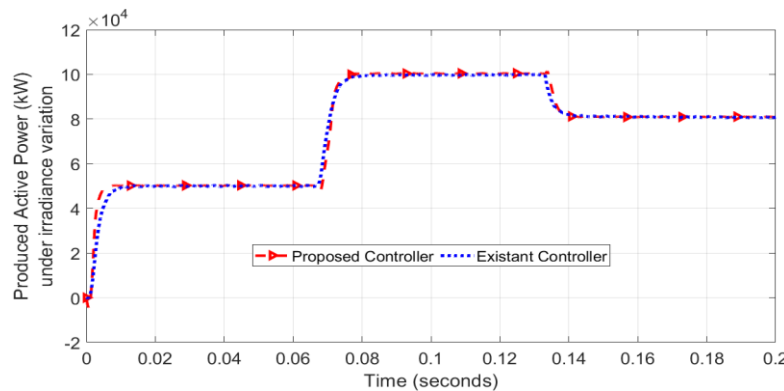


Figure 9. Active power delivered into the grid with changes in solar irradiance

3.3. Case 3: Controller performance in terms of maintaining power balance

The grid-connected photovoltaic system is connected to a three-phase load in this scenario. The load's maximum power is 70 kW, and its reactive power is 50 kVA. At the start of this simulation, it is assumed that the photovoltaic unit operates at 500 W/m² until $t = 0.1$ s as shown in Figure 10(a), implying that the photovoltaic unit's output power is 50 kW, and the load demand is 70 kW. As a result, the active power delivered to the load will be 50 kW, and the grid will supply 20 kW from the load, as shown in Figure 10(b).

During the time interval $t = 0.1$ s to $t = 0.2$ s, the solar irradiance varies from 500 to 1,000 W/m², which results in 100 kW output power from the PV unit while the load remains at 70 kW. As a result, the load absorbs 70 kW, and the remaining 30 kW is sent to the grid to maintain power balance, as illustrated in Figure 10. As can be seen, the photovoltaic unit's output power is 100 kW, the load demand is 70 kW, and the power transferred to the grid is 30 kW. As a result, the power balance in the system can be considered. Figure 11 depicts the reactive power shared between the grid, the load, and the PV system.

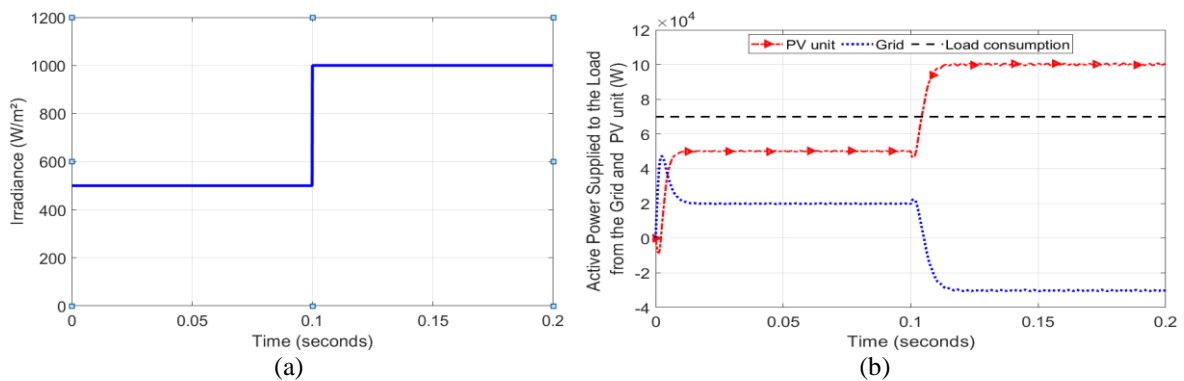


Figure 10. Power balance between PV source and the grid: (a) irradiation model and (b) active power delivered to the load from the grid and PV unit

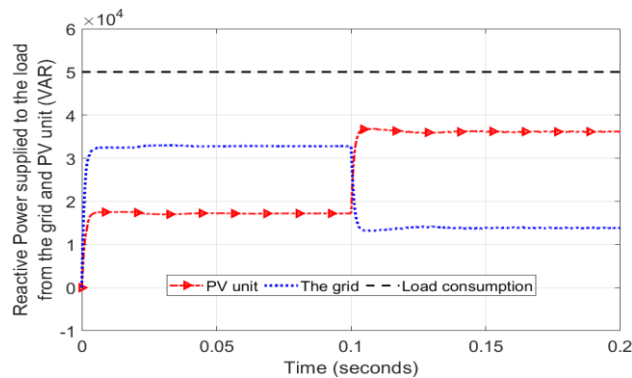


Figure 11. Reactive power sharing between PV source and the grid

4. CONCLUSION

In this paper, a novel backstepping controller based on DC link voltage control using a power balance method is designed to control the active and reactive power flow in a grid-connected solar PV system. The performance of the implemented controller is evaluated using numerical simulations in MATLAB/Simulink. The system continues to meet the overall objectives under various operating conditions for which it was developed, such as i) tracking the maximum power point, ii) controlling the DC link voltage at a given reference, and iii) injecting active and reactive power into the grid with lower harmonics.

As shown in the simulation results, the proposed backstepping controller performs satisfactorily in terms of improving power quality by reducing the THD of the current injected into the grid. It is also found that this controller is globally stable under changing atmospheric conditions as compared to the existing controller. The proposed controller can also ensure maximum power injection into the power grid under varying operating conditions by maintaining the power balance inside the grid-connected PV system.




REFERENCES

- [1] A. S. Anees, "Grid integration of renewable energy sources: Challenges, issues and possible solutions," in *2012 IEEE 5th India International Conference on Power Electronics (IICPE)*, Dec. 2012, pp. 1–6, doi: 10.1109/IICPE.2012.6450514.
- [2] F. Blaabjerg, Y. Yang, D. Yang, and X. Wang, "Distributed power-generation systems and protection," *Proceedings of the IEEE*, vol. 105, no. 7, pp. 1311–1331, Jul. 2017, doi: 10.1109/JPROC.2017.2696878.
- [3] T. Suntio and T. Messo, "Power electronics in renewable energy systems," *Energies*, vol. 12, no. 10, May 2019, doi: 10.3390/en12101852.
- [4] I.-S. Kim, "Robust maximum power point tracker using sliding mode controller for the three-phase grid-connected photovoltaic system," *Solar Energy*, vol. 81, no. 3, pp. 405–414, Mar. 2007, doi: 10.1016/j.solener.2006.04.005.
- [5] O. M. Arafa, A. A. Mansour, K. S. Sakkoury, Y. A. Atia, and M. M. Salem, "Realization of single-phase single-stage grid-connected PV system," *Journal of Electrical Systems and Information Technology*, vol. 4, no. 1, pp. 1–9, May 2017, doi: 10.1016/j.jesit.2016.08.004.
- [6] H. Li, Y. Xu, S. Adhikari, D. T. Rzy, F. Li, and P. Irminger, "Real and reactive power control of a three-phase single-stage PV system and PV voltage stability," in *2012 IEEE Power and Energy Society General Meeting*, Jul. 2012, pp. 1–8, doi: 10.1109/PESGM.2012.6343965.
- [7] A. Borni *et al.*, "Optimized MPPT controllers using GA for grid connected photovoltaic systems, comparative study," *Energy Procedia*, vol. 119, pp. 278–296, Jul. 2017, doi: 10.1016/j.egypro.2017.07.084.
- [8] N. Altin, S. Ozdemir, H. Komurcugil, I. Sefa, and S. Biricik, "Two-stage grid-connected inverter for PV systems," in *2018 IEEE 12th International Conference on Compatibility, Power Electronics and Power Engineering (CPE-POWERENG 2018)*, Apr. 2018, pp. 1–6, doi: 10.1109/CPE.2018.8372540.
- [9] S. I. Nanou, A. G. Papakonstantinou, and S. A. Papathanassiou, "A generic model of two-stage grid-connected PV systems with primary frequency response and inertia emulation," *Electric Power Systems Research*, vol. 127, pp. 186–196, Oct. 2015, doi: 10.1016/j.epsr.2015.06.011.
- [10] O. L. Santos, "Contribution to the DC-AC conversion in photovoltaic systems: Module oriented converters," University de Toulouse, 2015, doi: 10.13140/RG.2.1.3400.3368.
- [11] S. Kouro, J. I. Leon, D. Vinnikov, and L. G. Franquelo, "Grid-connected Photovoltaic systems: An overview of recent research and emerging PV converter technology," *IEEE Industrial Electronics Magazine*, vol. 9, no. 1, pp. 47–61, Mar. 2015, doi: 10.1109/MIE.2014.2376976.
- [12] A. Hoke and D. Maksimovic, "Active power control of photovoltaic power systems," in *2013 1st IEEE Conference on Technologies for Sustainability (SusTech)*, Aug. 2013, pp. 70–77, doi: 10.1109/SusTech.2013.6617300.
- [13] S. A. Azmi, M. F. N. Tajuddin, M. F. Mohamed, and L. J. Hwai, "Multi-loop control strategies of three-phase two-level current source inverter for grid interfacing photovoltaic system," in *2017 IEEE Conference on Energy Conversion (CENCON)*, Oct. 2017, pp. 277–282, doi: 10.1109/CENCON.2017.8262498.
- [14] K. Boudaraia, H. Mahmoudi, and M. El Azzaoui, "Modeling and control of three Phases grid connected photovoltaic system," in *International Renewable and Sustainable Energy Conference (IRSEC)*, 2016, pp. 812–816, doi: 10.1109/IRSEC.2016.7984004.
- [15] P. Gakhar and M. Gupta, "A novel control strategy for power quality improvement in grid-connected solar photovoltaic system," *Indonesian Journal of Electrical Engineering and Computer Science*, vol. 15, no. 3, pp. 1264–1272, Sep. 2019, doi: 10.11591/ijeecs.v15.i3.pp1264-1272.
- [16] A. Elallali, A. Abouloifa, I. Lachkar, C. Taghzaoui, F. Giri, and Y. Mchaouar, "Nonlinear control of grid-connected PV systems using active power filter with three-phase three-level NPC inverter," *IFAC-PapersOnLine*, vol. 55, no. 12, pp. 61–66, 2022, doi: 10.1016/j.ifacol.2022.07.289.
- [17] Y. Abouelmahjoub and M. Moutchou, "Nonlinear control strategy of single-phase unified power flow controller," *International Journal of Electrical and Computer Engineering (IJECE)*, vol. 11, no. 4, pp. 2864–2875, Aug. 2021, doi: 10.11591/ijece.v11i4.pp2864-2875.
- [18] D. Lalili, A. Mellit, N. Lourci, B. Medjahed, and E. M. Berkouk, "Input output feedback linearization control and variable step size MPPT algorithm of a grid-connected photovoltaic inverter," *Renewable Energy*, vol. 36, no. 12, pp. 3282–3291, Dec. 2011, doi: 10.1016/j.renene.2011.04.027.
- [19] T. Abderrahim, T. Abdelwahed, and M. Radouane, "Improved strategy of an MPPT based on the sliding mode control for a PV system," *International Journal of Electrical and Computer Engineering (IJECE)*, vol. 10, no. 3, pp. 3074–3085, Jun. 2020, doi: 10.11591/ijece.v10i3.pp3074-3085.
- [20] S.-A. Touil, N. Boudjerda, A. Boubakir, and A. Boudouda, "Sliding mode control of a grid-connected photovoltaic source via a three-phase inverter using incremental conductance MPPT," in *2017 5th International Conference on Electrical Engineering-Boumerdes (ICEE-B)*, Oct. 2017, pp. 1–6, doi: 10.1109/ICEE-B.2017.8192220.
- [21] C. Aouadi *et al.*, "Multi loop based control of photovoltaic system connected to the single phase grid," in *2016 International Renewable and Sustainable Energy Conference (IRSEC)*, Nov. 2016, pp. 479–483, doi: 10.1109/IRSEC.2016.7983961.
- [22] H. Bahri, M. Aboulfatah, M. Guisser, E. Abdelmounim, and M. El Malah, "Integral backstepping control for maximum power point tracking and unity power factor of a three phase grid connected photovoltaic system," *International Journal of Electrical and Computer Engineering (IJECE)*, vol. 7, no. 4, pp. 1671–1680, Aug. 2017, doi: 10.11591/ijece.v7i4.pp1671-1680.
- [23] M. Guisser, M. Aboulfatah, E. Abdelmounim, H. Medromi, and J. Saadi, "Nonlinear control design for Maximum power point tracking and unity power factor of a grid-connected photovoltaic renewable energy systems," *IOSR Journal of Electronics and Communication Engineering*, vol. 9, no. 5, pp. 62–71, 2014, doi: 10.9790/2834-09546271.
- [24] M. Merai, M. W. Naouar, I. Slama-Belkhdja, and E. Monmasson, "A systematic design methodology for DC-link voltage control of single phase grid-tied PV systems," *Mathematics and Computers in Simulation*, vol. 183, pp. 158–170, May 2021, doi: 10.1016/j.matcom.2020.05.007.
- [25] X. H. Nguyen and M. P. Nguyen, "Mathematical modeling of photovoltaic cell/module/arrays with tags in MATLAB/Simulink," *Environmental Systems Research*, vol. 4, no. 1, Dec. 2015, doi: 10.1186/s40068-015-0047-9.
- [26] S. Kasbi, E. Rijanto, and R. bin Abd Ghani, "Design and implementation of controller for boost DC-DC converter using PI-LPF based on small signal model," *Journal of Mechatronics, Electrical Power, and Vehicular Technology*, vol. 6, no. 2, pp. 105–112, Dec. 2015, doi: 10.14203/j.mev.2015.v6.105-112.
- [27] S. Roy, P. Kumar Sahu, S. Jena, and A. Kumar Acharya, "Modeling and control of DC/AC converters for photovoltaic grid-tie micro-inverter application," *Materials Today: Proceedings*, vol. 39, pp. 2027–2036, 2021, doi: 10.1016/j.matpr.2020.09.330.
- [28] E. Radwan, K. Salih, E. Awada, and M. Nour, "Modified phase locked loop for grid connected single phase inverter," *International Journal of Electrical and Computer Engineering (IJECE)*, vol. 9, no. 5, pp. 3934–3943, Oct. 2019, doi: 10.11591/ijece.v9i5.pp3934-3943.




- [29] A. Yahya, H. El Fadil, J. M. Guerrero, F. Giri, and H. Erguig, "Three-phase grid-connected of photovoltaic generator using nonlinear control," in *2014 IEEE Conference on Control Applications (CCA)*, Oct. 2014, pp. 879–884, doi: 10.1109/CCA.2014.6981447.

BIOGRAPHIES OF AUTHORS



Salwa Naddami    is a Ph.D. student. She received her B.Sc. degree in electrical engineering from the Science and Technical Faculty of Hassan 1st University, Settat, Morocco, in 2014, the M.Sc. degree in Automatic, Signal Processing and Industrial Computing from the Science and Technical Faculty of Hassan 1st University, Settat, Morocco, in 2017. Her current research interests include power electronics and the PV-wind hybrid renewable energy systems in the Laboratory of Mechanical Engineering, Industrial Management, and Innovation at Hassan 1st University. She can be contacted at s.naddami@uhp.ac.ma.



Najib Ababssi    was born in Rabat, Morocco, in 1962. He is a Dr. engineer in electrical engineering. His research interests include electrical networks. He is currently researcher professor at science and technical faculty, Hassan 1st University, Settat, Morocco. He can be contacted at nababssi@gmail.com.